The Astronomical Journal, 123:2070–2082, 2002 April


# THE *INFRARED SPACE OBSERVATORY* DEEP ASTEROID SEARCH[1]

Edward F. Tedesco
TerraSystems, Inc., 59 Wednesday Hill Road, Lee, NH 03824; etedesco@terrasys.com

and

François-Xavier Desert
Laboratoire d'Astrophysique, Observatoire de Grenoble, B.P. 53, 414 rue de la Piscine, F-38041 Grenoble Cedex 9, France;
Francois-Xavier.Desert@obs.ujf-grenoble.fr
*Received 2001 October 2; accepted 2002 January 2*

## ABSTRACT

A total of six deep exposures (using the astronomical observation template CAM01 with a 6″ pixel field of view) through the ISOCAM LW10 filter (*IRAS* band 1, i.e., 12 $\mu$m) were obtained on a $\sim$15′ square field centered on the ecliptic plane. Point sources were extracted using the technique described in 1999 by Désert et al. Two known asteroids appear in these frames, and 20 sources moving with velocities appropriate for main-belt asteroids are present. Most of the asteroids detected have flux densities less than 1 mJy, that is, between 150 and 350 times fainter than any of the asteroids observed by *IRAS*. These data provide the first direct measurement of the 12 $\mu$m sky-plane density for asteroids on the ecliptic equator. The median zodiacal foreground, as measured by ISOCAM during this survey, is found to be 22.1 $\pm$ 1.5 mJy pixel$^{-1}$, i.e., 26.2 $\pm$ 1.7 MJy sr$^{-1}$. The results presented here imply that the actual number of kilometer-sized asteroids may be higher than several recent estimates based upon observations at visual wavelengths and are in reasonable agreement with the statistical asteroid model. Using results from the observations presented here, together with three other recent population estimates, we conclude that the cumulative number of main-belt asteroids with diameters greater than 1 km is (1.2 $\pm$ 0.5) $\times$ $10^6$.

*Key words:* infrared radiation — minor planets, asteroids — solar system: general

*On-line material:* animation, machine-readable table

## 1. INTRODUCTION

Most main-belt asteroids are found between 2.1 and 3.3 AU from the Sun and at ecliptic latitudes less than 20°. Except for the largest asteroids (diameters greater than $\sim$30 km), the actual number above a given size is poorly known. For example, recent estimates of the number of main-belt asteroids with diameters larger than 1 km range from $\sim 3 \times 10^5$ (Evans et al. 1998) to $\sim 2 \times 10^6$ (Tedesco, Cellino, & Zappalà 2002a).

The asteroid size distribution is important because it provides constraints on models of the original size distribution of the planetesimals formed in the inner solar system and their subsequent evolution. It is also an important datum in modeling the numerical size of the population of near-Earth asteroids and accounting for their evolution from the main belt into Earth-orbit–crossing orbits.

A 1 km asteroid has a $V$ magnitude between 19 and 24 near opposition (corresponding to heliocentric distances of 2.1 and 3.3 AU and albedos of 0.36 and 0.03, respectively). It would be a straightforward program to survey, at visible wavelengths, all asteroids in given regions of the sky brighter than this limit. However, because for any given distance, visual surveys are biased in favor of discovering larger, higher albedo asteroids, magnitude data alone cannot be used to accurately derive asteroid *diameters*. This is because the absolute brightness of an asteroid depends upon its cross section and albedo, and asteroid albedos span a range of at least a factor of 12 ($\sim$95% of asteroids with *IRAS* albedos have values between 0.03 and 0.36). Moreover, there may be systematic trends of albedo with size (e.g., Tedesco 1994).

Observing thermal emission permits us to obtain an accurate distribution of asteroid diameters because, unlike the linear dependence with albedo at visual wavelengths, the infrared flux is only weakly dependent on the geometric albedo. For example, on 2001 March 26, the 100 km main-belt asteroid 50 Virginia was at a solar elongation of 110°, a typical elongation for space-based infrared observations. Virginia's visual magnitude at this time, given its SIMPS (Tedesco et al. 2002b) diameter of 99.82 km, would be 14.5 if its visual geometric albedo were 0.03, and 11.8 if its visual geometric albedo were 0.36, a difference of 2.7 mag. The 12.0 $\mu$m magnitudes under these same conditions would be 2.16 and 2.46, respectively, or a difference of only 0.3 mag. Furthermore, the lower albedo would actually result in a slightly higher 12.0 $\mu$m brightness because in this case the asteroid's temperature would be higher. Thus, an infrared survey is slightly biased in favor of discovering *lower albedo* asteroids.

To date, there have been three space-based infrared surveys in which asteroids have been incidentally observed: the *Infrared Astronomical Satellite* (*IRAS*), the *Midcourse Space Experiment* (*MSX*; Mill et al. 1994), and the *Infrared Space Observatory* (*ISO*) spacecraft, reported on here. For a description of the *ISO* mission, see Kessler et al. (1996), and for details on the ISOCAM instrument, see Cesarsky et al. (1996).

[1] Based on observations with the *Infrared Space Observatory* (*ISO*), an ESA project with instruments funded by ESA Member states (especially the PI countries: France, Germany, the Netherlands, and the UK) with the participation of ISAS and NASA.

Results on *IRAS* asteroids are given in Tedesco (1992)[2] and Tedesco et al. (2002b), and those on asteroids observed by *MSX* in Tedesco, Egan, & Price (2001).

The *IRAS* asteroid survey is severely incomplete at low flux levels, that is, below about 1 Jy, because *IRAS* could only detect an asteroid in its survey mode if a known orbit was available. Thus, although *IRAS* observed at infrared wavelengths, it was limited by the (albedo biased) visual surveys in which asteroids are discovered and from which data their orbits are calculated. Although *IRAS* knowingly discovered no main-belt asteroids, due primarily to the poor spatial resolution of its detectors, many unrecognized asteroid detections are still present in its point-source reject database. An example of this is the 432 multiply observed asteroids recently extracted by Tedesco et al. (2002b).

*IRAS* and *MSX* serendipitously observed numerous asteroids in the course of their nominal missions. However, because of the way in which their observations were conducted, only asteroids with known orbits were identified with the infrared sources these spacecraft detected. *IRAS* observed ~95% of the sky and *MSX* about 10%. Although the faintest asteroids detected in these surveys have flux densities of about 150 mJy, they are in no way complete to this flux level. The *ISO* asteroid search (discussed below) observed about 0.125 deg$^2$ of sky to a completeness limit of ~0.6 mJy.

[2] Available from S. D. Price, Space Vehicles Directorate, Air Force Research Laboratory, 29 Randolph Road, Hanscom AFB, MA 01731-3010; Steve.Price@hanscom.af.mil.

## 2. THE *ISO* DEEP ASTEROID SEARCH (IDAS)

The goal of this survey was to cover the maximum area of sky to the faintest flux limit possible under the constraints imposed by the zodiacal background and the available observing time. The field was selected to be in the ecliptic plane, near the upper limit of the *ISO* solar elongation constraint (i.e., near 106°), and located west of the Sun (to facilitate ground-based follow-up). In addition, the field was chosen to lie far from the Galactic plane and to contain no known *IRAS* sources or bright stars. The sensor used was *ISO*'s astronomical observation template CAM01 with a 6″ pixel field of view (PFOV) and using the ISOCAM LW10 filter (*IRAS* band 1, i.e., 12 $\mu$m).

Asteroids move, and their flux may vary appreciably on timescales as short as minutes. Consequently, the exposure time was chosen to freeze asteroid motion on each submap, where a submap is a $3' \times 3'$ area (the size of the ISOCAM array) in which each inertial point was observed three times. Each submap consisted of a 30 s exposure sequence[3] at a

[3] A "clean" was performed at the start of each map. This flashed the array to remove the memory of the previous observation and required about 240 s. Next, 25 stabilization frames were taken. The actual observations consisted of four 5 s exposures at each point in the raster, plus an average of 10 s to step to the next raster position.

| | | | | | | | | | | | | | | | | | | |
|---|---|---|---|---|---|---|---|---|---|---|---|---|---|---|---|---|---|---|
| 1 | 2 | 3 | 3 | 3 | 3 | 3 | 3 | 3 | 3 | 3 | 3 | 3 | 3 | 3 | 3 | 3 | 2 | 1 |
| 2 | 4 | 6 | 6 | 6 | 6 | 6 | 6 | 6 | 6 | 6 | 6 | 6 | 6 | 6 | 6 | 6 | 4 | 2 |
| 3 | 6 | 9 | 9 | 9 | 9 | 9 | 9 | 9 | 9 | 9 | 9 | 9 | 9 | 9 | 9 | 9 | 6 | 3 |
| 3 | 6 | 9 | 9 | 9 | 9 | 9 | 9 | 9 | 9 | 9 | 9 | 9 | 9 | 9 | 9 | 9 | 6 | 3 |
| 3 | 6 | 9 | 9 | 9 | 9 | 9 | 9 | 9 | 9 | 9 | 9 | 9 | 9 | 9 | 9 | 9 | 6 | 3 |
| 3 | 6 | 9 | 9 | 9 | 9 | 9 | 9 | 9 | 9 | 9 | 9 | 9 | 9 | 9 | 9 | 9 | 6 | 3 |
| 3 | 6 | 9 | 9 | 9 | 9 | 9 | 9 | 9 | 9 | 9 | 9 | 9 | 9 | 9 | 9 | 9 | 6 | 3 |
| 3 | 6 | 9 | 9 | 9 | 9 | 9 | 9 | 9 | 9 | 9 | 9 | 9 | 9 | 9 | 9 | 9 | 6 | 3 |
| 3 | 6 | 9 | 9 | 9 | 9 | 9 | 9 | 9 | 9 | 9 | 9 | 9 | 9 | 9 | 9 | 9 | 6 | 3 |
| 3 | 6 | 9 | 9 | 9 | 9 | 9 | 9 | 9 | 9 | 9 | 9 | 9 | 9 | 9 | 9 | 9 | 6 | 3 |
| 3 | 6 | 9 | 9 | 9 | 9 | 9 | 9 | 9 | 9 | 9 | 9 | 9 | 9 | 9 | 9 | 9 | 6 | 3 |
| 3 | 6 | 9 | 9 | 9 | 9 | 9 | 9 | 9 | 9 | 9 | 9 | 9 | 9 | 9 | 9 | 9 | 6 | 3 |
| 3 | 6 | 9 | 9 | 9 | 9 | 9 | 9 | 9 | 9 | 9 | 9 | 9 | 9 | 9 | 9 | 9 | 6 | 3 |
| 3 | 6 | 9 | 9 | 9 | 9 | 9 | 9 | 9 | 9 | 9 | 9 | 9 | 9 | 9 | 9 | 9 | 6 | 3 |
| 3 | 6 | 9 | 9 | 9 | 9 | 9 | 9 | 9 | 9 | 9 | 9 | 9 | 9 | 9 | 9 | 9 | 6 | 3 |
| 3 | 6 | 9 | 9 | 9 | 9 | 9 | 9 | 9 | 9 | 9 | 9 | 9 | 9 | 9 | 9 | 9 | 6 | 3 |
| 3 | 6 | 9 | 9 | 9 | 9 | 9 | 9 | 9 | 9 | 9 | 9 | 9 | 9 | 9 | 9 | 9 | 6 | 3 |
| 2 | 4 | 6 | 6 | 6 | 6 | 6 | 6 | 6 | 6 | 6 | 6 | 6 | 6 | 6 | 6 | 6 | 4 | 2 |
| 1 | 2 | 3 | 3 | 3 | 3 | 3 | 3 | 3 | 3 | 3 | 3 | 3 | 3 | 3 | 3 | 3 | 2 | 1 |

FIG. 1.—Sample region coverage of a 17 × 17 raster map. Each $1' \times 1'$ cell shows the total number of 20 s integration sets made on that area. Each cell contains ~100 ISOCAM pixels. The square at the top right shows the size of the ISOCAM array.

fixed position followed by a step of 1′ in ecliptic longitude or latitude wherein the exposure sequence was repeated and ending with another 1′ step in ecliptic longitude or latitude where the exposure sequence was again repeated. The total time spent doing each point in a submap was 90 s. Because the apparent rate of motion for main-belt asteroids, under the observing geometry described above, is between 0″ and 60″ $hr^{-1}$, the maximum angular distance moved during the time required to obtain a submap is less than 1″.5. However, each submap was sampled three times to create the complete map, and the times between successive submaps varied from 30 to 870 s. Thus, the maximum distance a main-belt asteroid would move between samples of a given inertial point in the map is 14″.5.

Figure 1 is a schematic diagram of the map coverage. Each box is 1′ on a side, with north up and east to the right. The raster began with the 3′ × 3′ array located in the northeast corner of the map, as indicated by the heavy lines around the nine cells in the top right of the figure. One exposure sequence was made at this position, and then the array was moved 1′ (cell) west. Seventeen exposure sequences were made along a line of constant ecliptic latitude. This brought the array to the end of the first row. At this point, it stepped south 1′, made an exposure sequence at this position, and then made 16 steps of 1′ to the east to complete the second row. This process was then repeated until the center of the array had scanned 17 rows.

See the movie for an animated version of this figure speeded up by a factor of about 60. As can be seen from the movie, or the numbers in the figure, each cell around the outer 1′ of the map received no more than three exposure sequences, and those in the 1′ border interior to this region, no more than six. All other cells in the map received nine exposure sequences, for a total of 180 seconds each. We refer to the region with nine exposure sequences as the region of complete coverage.

The 15 × 15 raster map was obtained in the same way but using 15 instead of 17 steps. The complete coverage area is 15′ square for the maps obtained with the 17 × 17 raster and 13 ′ square for those obtained with the 15 × 15 raster.

Two maps as described above were made in 1996 June, and another four in 1997 June. A total of 13.64 hr were expended in obtaining the observations presented herein. Maps 1, 2, 5, and 6 required 2.44 hr per map, while maps 3 and 4 had available 1.94 hr each. A consequence of the decision to keep the exposure per map point constant over all six maps was that maps 3 and 4 (the 15 × 15 rasters) cover less area than the others.

The intention was to have maps 3 and 4 (the time for which was granted under a supplemental observing request) made at least 36 hr after the end of the previous map pair. However, they were scheduled less than 12 hr after completion of the previous map, and by the time the observing schedule was issued, it was too late to reschedule them.

The sample consists of six data sets that are now in the public domain[4] labeled as target dedicated time (TDT) numbers: 21103003, 21103004, 57200101, 57200102, 57200407, and 57200408 (corresponding respectively to maps 1, 2, 3, 4, 5, and 6 in Table 1). Thus, they were taken in pairs during two 24 hr *ISO* orbits (the first three digits in the TDT) separated by approximately 1 yr on 1996 June 15 and 1997 June 10 (i.e., on Julian Dates 2,450,249 and 2,450,609, respectively).

Figure 2 shows the six images obtained after processing using the technique of Désert et al. (1999), which is further described in § 3. Figure 3 shows all point sources with a signal-to-noise ratio (S/N) of 3.0 extracted from the ISOCAM maps shown in Figure 2. Squares outline the areas sampled nine times. The point size is proportional to the flux density, which ranges from 0.28 to 12.2 mJy.

## 3. ISOCAM DATA REDUCTION

### 3.1. *Observation Characteristics*

A typical data set consists of 1800 readouts, each with 5.1 s of integration, through the ISOCAM LW10 filter centered at 12 μm with a bandpass very similar to the *IRAS* 12 μm band. The lens wheel was on the LGe6 position, providing a ratio of 6″ per detector pixel (which is also close to the FWHM of the Airy pattern of *ISO*). The camera detector consists of 32 × 32 pixels, with one column (No. 24, disconnected before launch) missing, providing a 3′.2 × 3′.2 instantaneous field of view. The total survey area was covered by making a raster with *ISO* at positions on a 17 × 17 (or 15 × 15) grid with 60″ (10 pixel) steps and 60″ line separation. Each position was observed for four readouts, i.e., 20 s of integration time. With the survey redundancy (a factor of 9), the total integration time per sky pixel is about 3 minutes. The median zodiacal foreground, as measured by ISOCAM during this survey, is found to be 22.1 ± 1.5 mJy $pixel^{-1}$, i.e., 26.2 ± 1.7 MJy $sr^{-1}$ (the error bar being the dispersion among the six surveys of the same area).

[4] See http://www.iso.vilspa.esa.es/.

TABLE 1

MAP FIELD CENTERS

| Map | R.A. (J2000.0) | Decl. (J2000.0) | Raster | Ecliptic Longitude J2000.0 Equinox | Ecliptic Latitude J2000.0 Equinox |
|---|---|---|---|---|---|
| 1......... | 22 08 38.6 | −08 34 10.4 | 17 × 17 | 338.000000 | 0.002471 |
| 2......... | 22 08 42.5 | −08 33 52.1 | 17 × 17 | 338.016800 | 0.001180 |
| 3......... | 22 08 38.6 | −08 34 10.4 | 15 × 15 | 338.000000 | 0.002471 |
| 4......... | 22 08 41.6 | −08 33 56.4 | 15 × 15 | 338.012900 | 0.001483 |
| 5......... | 22 08 38.6 | −08 34 10.4 | 17 × 17 | 338.000000 | 0.002471 |
| 6......... | 22 08 42.5 | −08 33 52.1 | 17 × 17 | 338.016800 | 0.001180 |

NOTE.—Units of right ascension are hours, minutes, and seconds, and units of declination are degrees, arcminutes, and arcseconds.

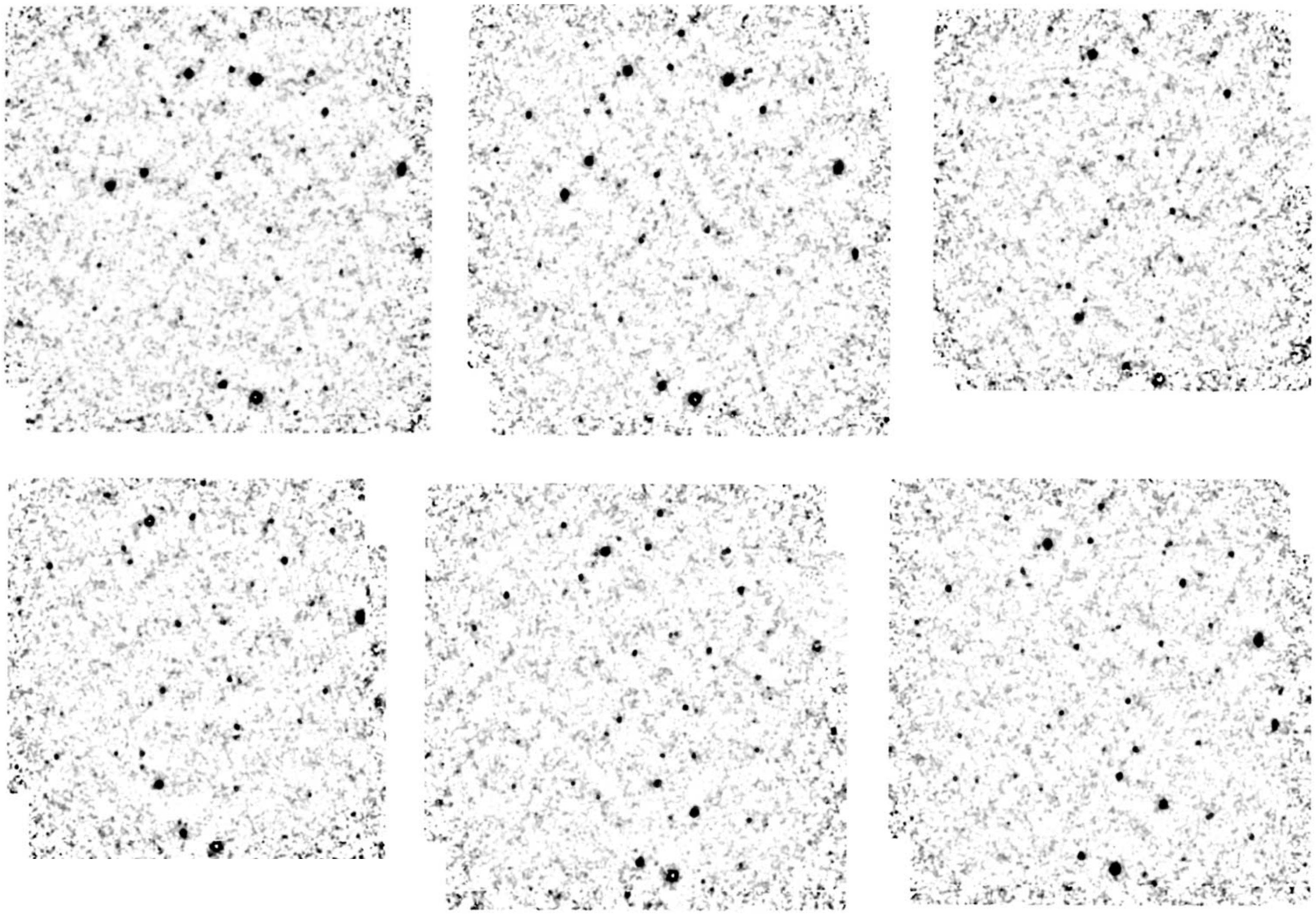

FIG. 2.—ISOCAM maps in ecliptic coordinates: (*top left two panels*) 1996 June 15 and (*all other panels* ) 1997 June 10. North ecliptic latitude is up, and east ecliptic longitude is to the right. The larger maps are $17 \times 17$ rasters, while the smaller maps are $15 \times 15$ rasters.

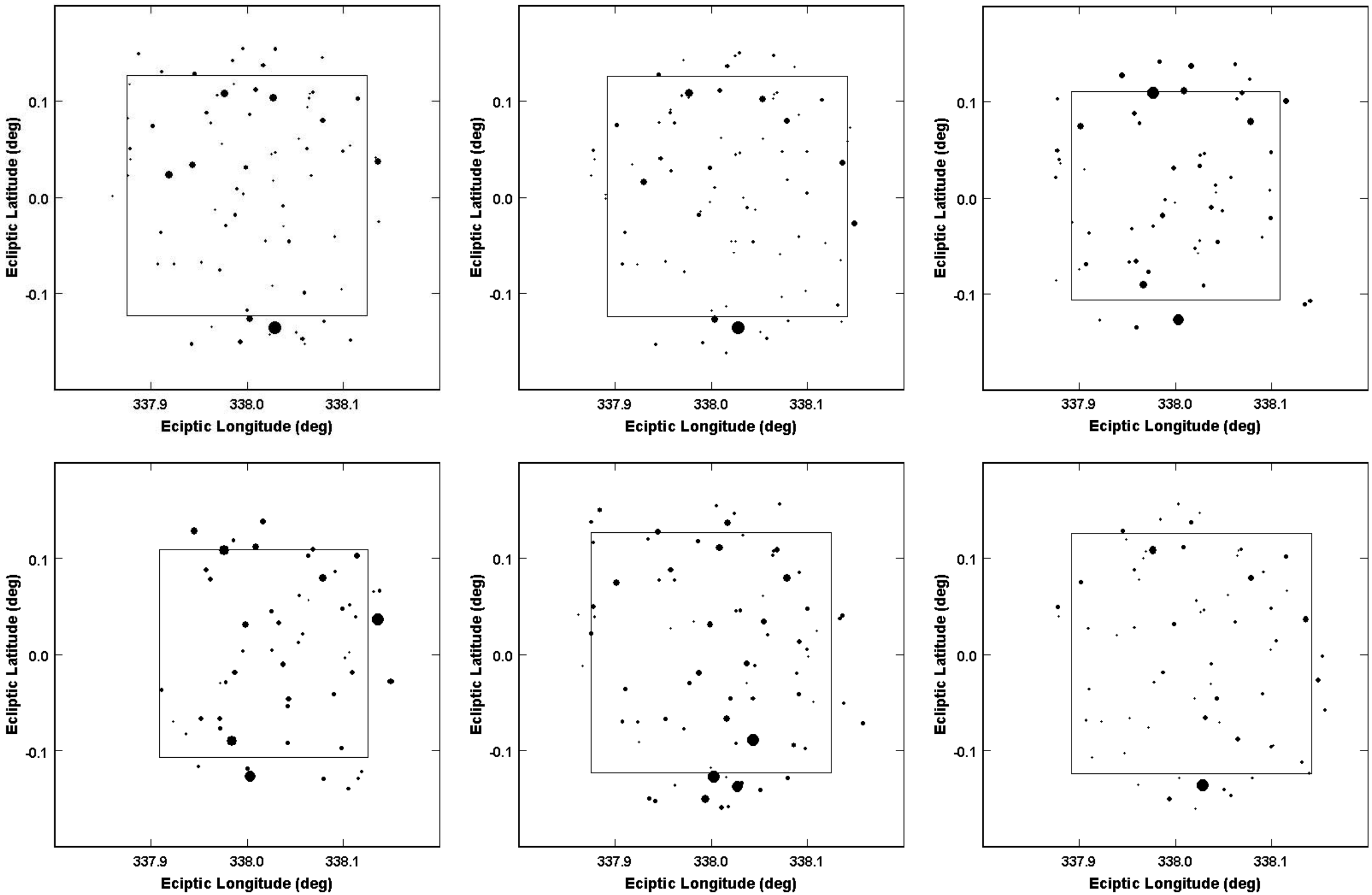


FIG. 3.—Point sources from the ISOCAM maps shown in Fig. 2. Squares outline the areas sampled nine times. The point size is proportional to the flux density, which ranges from 0.28 to 12.2 mJy.

### 3.2. *Summary of Data Reduction*

The raw data consists of a cube (CISP files) of detector readouts (one every 36 CAM time units, i.e., 5.1 s) and an *ISO* pointing history (IIPH) file. The detailed data reduction procedure is described by Désert et al. (1999). Here we give a summary, along with the specific parameters that were used for the present data sets. First, cosmic rays are removed by a time-line analysis of each pixel. Long duration glitches are also removed and a transient correction applied, using the method described by Coulais & Abergel (2000).

The data time line is then analyzed with a "triple beam" linear algorithm that basically finds, for each camera pixel, the difference between the signal at one raster position and the average of the two adjacent position signals. The dispersion of this difference for different raster positions indicate the true pixel noise of the measurements because, most of the time, it is uncontaminated by sources. Badly behaved pixel values (due to glitches and bad triple-beam $\chi^2$) are discarded by an adapted $\sigma$-clipping. We project the difference and dispersion on a final sky map, using neighbor pixel approximation, with a 2″ pixel size. A redundancy number is also obtained this way. The projection is done by co-adding with an optimal weighing and a first-order array distortion correction. We used the associations with the USNO optical catalog (version A2.0; Monet et al. 1998)[5] to deduce the offset positions (up to 7″ in both directions) to apply to each data set map (because of the so-called lens filter wheel jitter).

The final map is then searched for point sources in a selected area where the redundancy is two or more. As explained by Désert et al. (1999), we iterate an algorithm where a candidate source (found with a top-hat wavelet) is fitted with a 9″ FWHM two-dimensional Gaussian (for the position and intensity), and the fit is removed. This algorithm allows measuring source fluxes near undefined pixels without underestimating the flux (as aperture photometry would do). The noise in the flux measurement is deduced from the noise map and the Gaussian least-square fitting algorithm. The absolute fluxes were deduced using the nominal ISOCAM internal unit to millijansky conversion factor (i.e., by assuming that the factor has not changed with respect to preflight calibration) and by applying a correction factor (1.52) to go from our fitted Gaussian beam flux to total point-spread function integrated flux.

In Table 2, we give the complete catalog of (527) sources that were detected at the $\geq 3\ \sigma$ level in any of the six maps. Column (1) is an identification number; columns (2) and (3), the J2000.0 right ascension and declination; column (4), the flux density in band LW10; column (5), the 1 $\sigma$ uncertainty in the flux density; column (6), the signal-to-noise ratio; columns (7)–(9), quality flags; column (10), the Julian Date of the observation (an average of the up to nine measurements on each point source that are available); column (11), a confusion flag; and column (12), a code indicating whether the source was in the multiply sampled region. Columns (13)–(19) provide data on sources found within 6″ of a USNO-A2.0 catalog (Monet et al. 1998) visible source.[6] Column (13) gives the red magnitude from the USNO-A2.0 catalog; column (14), the name from USNO-A2.0; column (15), the number of USNO-A2.0 sources associated with the *ISO* source; column (16), the number from the USNO-A2.0 catalog; column (17), the distance from the USNO-A2.0 catalog source (95% are within 4″); and columns (18) and (19), the distances in right ascension and declination, respectively, from the USNO A2.0 catalog source, rounded to the nearest arcsecond.

A catalog of 63 inertial sources is given in Table 3 and plotted in Figure 4. These are sources from Table 2 that are

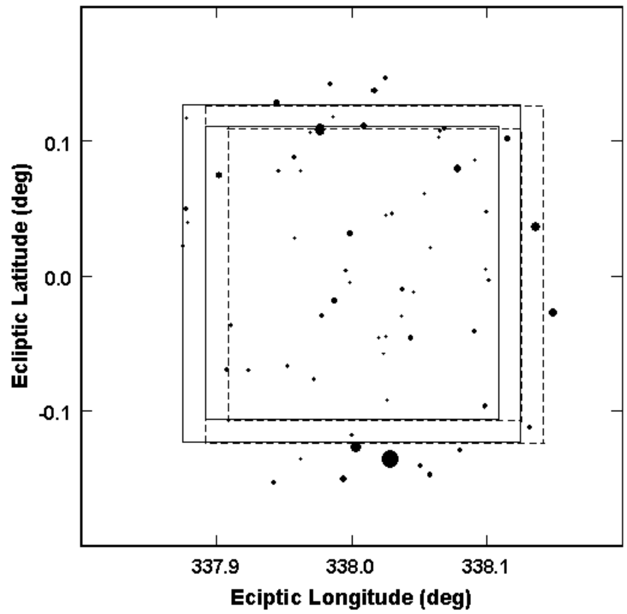


FIG. 4.—IDAS inertial point sources. Squares outline the areas sampled nine times per map. The inertial sky within the union of the two large squares was sampled 36 times (total integration time 720 s per map pixel) and that within the two small squares 54 times (total integration time 1080 s per map pixel). The point size is proportional to the flux density, which ranges from 0.34 to 10.8 mJy.

[5] Available at http://ftp.nofs.navy.mil/projects/pmm/catalogs.html.

[6] As reduced by CDS/VizieR, http://cdsweb.u-strasbg.fr/CDS.html.

TABLE 2

ALL POINT SOURCES EXTRACTED FROM THE SIX IDAS MAPS

| ID (1) | R.A. (2) | Decl. (3) | FD (4) | $\sigma$ (5) | S/N (6) | Q1 (7) | Q2 (8) | Q3 (9) | JD (10) | G (11) | C (12) | $R$ (13) | USNO Name (14) | Associations (15) | No. (16) | $D$ (17) | $D_{R.A.}$ (18) | $D_{decl.}$ (19) |
|---|---|---|---|---|---|---|---|---|---|---|---|---|---|---|---|---|---|---|
| 0...... | 339.739269 | −8.684638 | 9528 | 247 | 38.6 | 0 | 1 | 4 | 249.78064 | 1 | 0 | 99.9 | 0750-21274627 | 1 | 362 | 1.9 | −2 | −1 |
| 1...... | 339.598482 | −8.477787 | 3687 | 164 | 22.4 | 0 | 1 | 4 | 249.78499 | 1 | 1 | 10.6 | 0750-21272024 | 1 | 183 | 3.0 | −3 | 1 |
| 2...... | 339.711469 | −8.685792 | 3163 | 134 | 23.6 | 0 | 1 | 4 | 249.78324 | 1 | 1 | 0.0 | ... | 0 | 0 | −1.0 | 0 | 0 |
| 3...... | 339.575977 | −8.577812 | 3520 | 140 | 25.1 | 1 | 1 | 4 | 249.79034 | 1 | 1 | 0.0 | ... | 0 | 0 | −1.0 | 0 | 0 |
| 4...... | 339.647069 | −8.463253 | 3767 | 171 | 22.0 | 0 | 4 | 4 | 249.78111 | 1 | 1 | 0.0 | ... | 0 | 0 | −1.0 | 0 | 0 |

NOTE.—Table 2 is presented in its entirety in the electronic edition of the Astronomical Journal. A portion is shown here for guidance regarding its form and content.

TABLE 3

IDAS Field Inertial Point Sources

| ID | R.A. | Decl. | FD | $\sigma$ | S/N | $R$ | USNO Name | Associations |
|---|---|---|---|---|---|---|---|---|
| 0...... | 339.502145 | −8.506749 | 407 | 67 | 6.0 | . . . | . . . | 146, 8096 |
| 1...... | 339.527498 | −8.568980 | 849 | 52 | 16.2 | 18.9 | 0750-21270670 | 79, 1017, 4008, 8037, 9022 |
| 2...... | 339.532663 | −8.578120 | 450 | 45 | 10.0 | 13.3 | 0750-21270745 | 115, 1085, 4034, 8103, 9069 |
| 3...... | 339.535786 | −8.595465 | 479 | 59 | 8.2 | 13.5 | 0750-21270820 | 103, 1099, 4169, 8034 |
| 4...... | 339.540586 | -8.536923 | 1499 | 44 | 33.9 | . . . | . . . | 17, 1007, 4003, 8008, 9006 |
| 5...... | 339.561057 | −8.471207 | 1254 | 62 | 20.1 | 17.5 | 0750-21271301 | 14, 1023, 4007, 5069, 8009, 9009 |
| 6...... | 339.580975 | −8.517697 | 565 | 72 | 7.9 | . . . | . . . | 1270, 8152 |
| 7...... | 339.587977 | −8.503622 | 885 | 42 | 21.0 | 14.7 | 0750-21271831 | 32, 1056, 4017, 5020, 8019, 9044 |
| 8...... | 339.590961 | −8.636819 | 604 | 40 | 15.1 | 13.7 | 0750-21271877 | 36, 1045, 4048, 5104, 8075, 9034 |
| 9...... | 339.592123 | −8.482400 | 536 | 51 | 10.5 | . . . | . . . | 143, 1132, 9274 |
| 10.... | 339.592687 | −8.443355 | 747 | 119 | 6.3 | . . . | . . . | 76, 4011 |
| 11.... | 339.596250 | −8.511510 | 663 | 42 | 15.7 | . . . | . . . | 109, 1071, 4056, 5031, 8191, 9120 |
| 12.... | 339.598123 | −8.477542 | 4867 | 86 | 56.3 | 10.6 | 0750-21272024 | 1, 1000, 4001, 5001, 9001 |
| 13.... | 339.600250 | −8.668321 | 637 | 43 | 14.8 | 19.1 | 0750-21272064 | 44, 1069, 4021, 8048, 9063 |
| 14.... | 339.603519 | −8.465211 | 580 | 63 | 9.3 | . . . | . . . | 241, 5041, 8047 |
| 15.... | 339.611103 | −8.559631 | 429 | 56 | 7.7 | . . . | . . . | 1125, 8253, 9107 |
| 16.... | 339.615798 | −8.662995 | 416 | 42 | 10.0 | . . . | . . . | 215, 1169, 5198, |
| 17.... | 339.625113 | −8.436006 | 1342 | 55 | 24.5 | 16.2 | 0750-21272521 | 15, 1013, 4010, 5009, 8017, 9028 |
| 18.... | 339.627154 | −8.462892 | 1659 | 50 | 33.5 | 11.5 | 0750-21272547 | 7, 1006, 4002, 5010, 8007, 9008 |
| 19.... | 339.628997 | −8.423933 | 564 | 91 | 6.2 | . . . | . . . | 1080, 8044, 9142, |
| 20.... | 339.641625 | −8.649331 | 623 | 45 | 13.8 | . . . | . . . | 134, 1053, 4080, 5025, 8023, 9098 |
| 21.... | 339.648022 | −8.541135 | 1373 | 47 | 29.2 | . . . | . . . | 13, 1011, 4091, 5007, 8015, 9012 |
| 22.... | 339.651048 | −8.605006 | 603 | 46 | 13.1 | . . . | . . . | 55, 4149, 5126, 8058, 9054 |
| 23.... | 339.655479 | −8.567884 | 417 | 65 | 6.4 | . . . | . . . | 236, 5219 |
| 24.... | 339.656071 | −8.591558 | 1082 | 45 | 24.1 | 12.8 | 0750-21273104 | 21, 1018, 4009, 5019, 8012, 9018 |
| 25.... | 339.661912 | −8.574583 | 384 | 74 | 5.2 | 18.8 | 0750-21273204 | 1191, 4131 |
| 26.... | 339.663695 | −8.651154 | 601 | 42 | 14.4 | 18.9 | 0750-21273242 | 125, 1059, 4038, 5076, 9104 |
| 27.... | 339.664282 | −8.732838 | 834 | 111 | 7.5 | 18.3 | 0750-21273245 | 123, 1026, 8067 |
| 28.... | 339.668283 | −8.518580 | 510 | 40 | 12.7 | 14.7 | 0750-21273317 | 136, 1121, 4170, 5046, 8073, 9139 |
| 29.... | 339.671654 | −8.515432 | 523 | 44 | 11.9 | . . . | . . . | 114, 1118, 4062, 8107, 9047 |
| 30.... | 339.676826 | −8.709590 | 410 | 70 | 5.9 | . . . | . . . | 131, 8192, 9072 |
| 31.... | 339.681931 | −8.445261 | 441 | 45 | 9.8 | 18.6 | 0750-21273599 | 185, 1057, 8072, 9092 |
| 32.... | 339.682437 | −8.450058 | 497 | 46 | 10.8 | 19.0 | 0750-21273607 | 180, 1117, 4077, 5165, 8199, 9058 |
| 33.... | 339.684090 | −8.442555 | 869 | 44 | 19.6 | 18.6 | 0750-21273647 | 81, 1038, 4012, 5030, 8022, 9067 |
| 34.... | 339.688585 | −8.492524 | 442 | 41 | 10.7 | . . . | . . . | 130, 1065, 5111, 8197, 9176 |
| 35.... | 339.697056 | −8.604695 | 508 | 47 | 10.9 | 19.7 | 0750-21273857 | 135, 1179, 8027, 9284 |
| 36.... | 339.699698 | −8.564683 | 1020 | 37 | 27.4 | 12.8 | 0750-21273912 | 18, 1029, 4015, 5008, 8011, 9020 |
| 37.... | 339.702035 | −8.602145 | 406 | 79 | 5.1 | . . . | . . . | 1184, 4207 |
| 38.... | 339.704640 | −8.466331 | 2166 | 48 | 45.4 | 18.5 | 0750-21274005 | 6, 1004, 4004, 5005, 8006, 9002 |
| 39.... | 339.704964 | −8.614536 | 340 | 72 | 4.7 | . . . | . . . | 1277, 4078 |
| 40.... | 339.705753 | −8.679018 | 520 | 54 | 9.6 | . . . | . . . | 51, 1167, 5058, 8095 |
| 41.... | 339.707689 | −8.528508 | 465 | 59 | 7.9 | . . . | . . . | 4033, 5150, 8134 |
| 42.... | 339.707062 | −8.583767 | 378 | 60 | 6.3 | . . . | . . . | 217, 8082, 9153 |
| 43.... | 339.708279 | −8.563930 | 473 | 65 | 7.3 | . . . | . . . | 1164, 8261 |
| 44.... | 339.711638 | −8.711600 | 1928 | 181 | 10.7 | 16.4 | 0750-21274141 | 19, 8030, 9014 |
| 45.... | 339.711796 | −8.686091 | 3937 | 69 | 56.7 | . . . | . . . | 2, 1002, 4000, 5000, 8000 |
| 46.... | 339.714394 | −8.455913 | 464 | 50 | 9.2 | 15.5 | 0750-21274181 | 1233, 5191, 8126, 9324, |
| 47.... | 339.719062 | −8.596113 | 964 | 45 | 21.2 | 12.2 | 0750-21274288 | 30, 1022, 4036, 5016, 8032, 9026 |
| 48.... | 339.720638 | −8.645489 | 450 | 65 | 6.9 | 13.6 | 0750-21274307 | 261, 8104 |
| 49.... | 339.730426 | −8.432215 | 1212 | 62 | 19.6 | 18.6 | 0750-21274495 | 12, 1014, 4006, 5011, 9019, |
| 50.... | 339.736522 | −8.488266 | 679 | 44 | 15.6 | . . . | . . . | 41, 1046, 4023, 5088, 8088, 9042 |
| 51.... | 339.739081 | −8.684950 | 10822 | 179 | 60.6 | 99.9 | 0750-21274627 | 0, 1001, 9000 |
| 52.... | 339.752527 | −8.528036 | 416 | 51 | 8.2 | . . . | . . . | 1194, 8215, 9196 |
| 53.... | 339.757206 | −8.534375 | 424 | 70 | 6.1 | . . . | . . . | 5122, 8092 |
| 54.... | 339.761885 | −8.680850 | 655 | 68 | 9.7 | . . . | . . . | 50, 1051, 8021, 9048 |
| 55.... | 339.761725 | −8.573803 | 636 | 42 | 15.0 | 17.8 | 0750-21275058 | 64, 1104, 4143, 5054, 8052, 9032 |
| 56.... | 339.770798 | −8.684376 | 1073 | 112 | 9.6 | . . . | . . . | 22, 1027, 9017 |
| 57.... | 339.774642 | −8.485023 | 3313 | 107 | 31.0 | 16.8 | 0750-21275320 | 9, 1009, 5003, 9003, |
| 58.... | 339.784544 | −8.659310 | 666 | 52 | 12.9 | . . . | . . . | 45, 1047, 5029, 8071, 9073 |
| 59.... | 339.790028 | −8.621748 | 620 | 64 | 9.6 | . . . | . . . | 152, 9103 |
| 60.... | 339.790029 | −8.623324 | 479 | 58 | 8.2 | . . . | . . . | 1239, 5036, 8155 |
| 61.... | 339.810757 | −8.539094 | 2225 | 92 | 24.2 | 13.5 | 0750-21275982 | 1005, 5017, 9007 |
| 62.... | 339.826604 | −8.624449 | 766 | 69 | 11.1 | 18.3 | 0750-21276278 | 1019, 9039 |

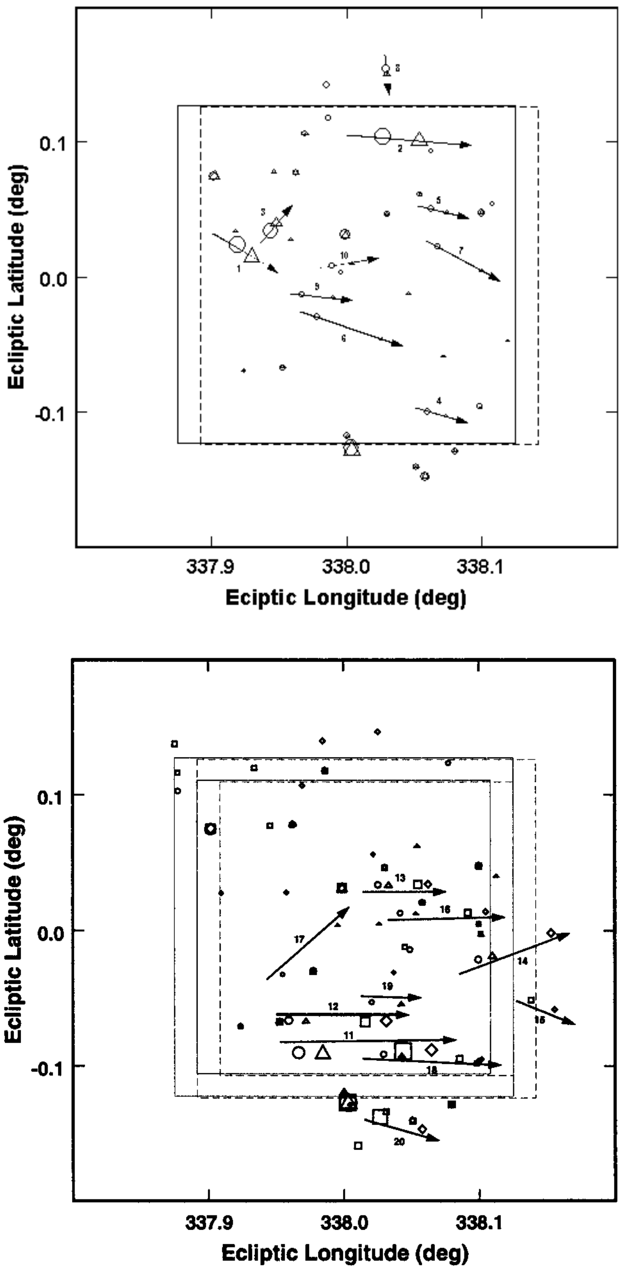


FIG. 5.—IDAS noninertial point sources, i.e., all sources from Fig. 3 not plotted in Fig. 4. Sources from the 1996 field are plotted in the top panel and those from the 1997 field in the bottom panel. Squares outline the areas sampled nine times per map. The symbol size is proportional to the flux density, which ranges from 0.43 to 5.7 mJy. Circles indicate sources extracted from map 1 (*top*) or 3 (*bottom*), triangles those from map 2 (*top*) or 4 (*bottom*), squares those from map 5, and diamonds those from map 6. Tracks are indicated by arrows through, or in crowded areas, parallel to, the data points.

seen at the same position in at least two maps. An average flux, ranging from 0.34 to 10.8 mJy, and error is given, along with the USNO-A2.0 catalog association. Some well-detected sources have no optical counterparts. These are probably external galaxies or very slow moving asteroids.

The complete (i.e., multiply observed) survey area is 225 arcmin$^2$ (0.0625 deg$^2$). The densities of stars and galaxies (assuming all non–USNO-A2.0 sources are galaxies), respectively, are found to be $0.072 \pm 0.017$ and $0.045 \pm 0.013$ arcmin$^{-2}$, for 12 $\mu$m flux densities greater than 0.6

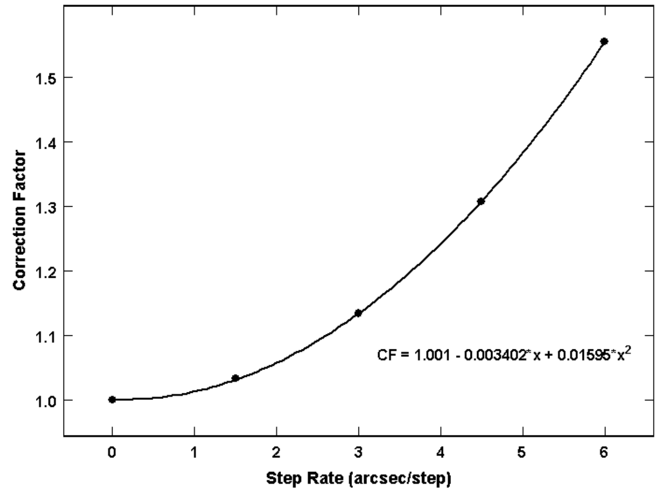


FIG. 6.—Moving-source flux correction

mJy (a value close to the 4 $\sigma$ level, where $\sigma$ is the median flux error in the complete area for one data set).

## 4. ASTEROID IDENTIFICATION

### 4.1. *IDAS Asteroids*

Moving sources were searched for in those areas observed in common within a day of each other. Twenty objects were found to move significantly (i.e., by more than 6″ over a period $\geq$2 hr). Figure 5 shows all sources from Figure 3 not plotted in Figure 4.

Because asteroids are moving sources, the technique described in § 3.2 for obtaining the flux from co-added images underestimates their flux. Thus, we derived a rate-of-motion dependent correction factor (FDCor) by offsetting the inertial sources by different amounts to simulate their motion and then performing the photometry as normally on the co-added map. This resulted in smaller flux values as a function of the amount offset, to which we fitted a second-order polynomial (shown in Fig. 6), viz.,

$$\mathrm{FDCor} = 1.001 - 0.0034x + 0.0160x^2 , \qquad (1)$$

where $x = \mathrm{RT} \times 30 \times$ rate and RT = 17 (for a $17 \times 17$ raster) or 15 (for a $15 \times 15$ raster), 30 is the time per sample, and the rate is the apparent rate of motion in arcseconds per revisit interval.

Table 2 contains the uncorrected flux densities, and Table 4, which presents the data on the 20 sources identified as being asteroids on the basis of forming tracks with two or more sightings, gives FDCor and the corrected flux densities, ranging from 0.43 to 5.7 mJy, for each sighting.

All of the identified asteroids have S/N > 4. The 1996 field contains four tracks in which at least one sighting has a flux density FD > 1 mJy, and the 1997 field contains six such tracks. Each field contains 10 tracks, in which at least one source has FD > 0.6 mJy, the 4 $\sigma$ completeness limit.

Combining the results from the two fields gives $5 \pm 1$ probable asteroids with FD > 1 mJy and $10 \pm 2$ with FD > 0.6 mJy, where the $\pm 2$ is an estimate, since the same number of tracks were in the two fields sampled a year apart.

Normalizing these results gives $80 \pm 16$ asteroids with FD > 1 mJy deg$^{-2}$ at the ecliptic plane and $160 \pm 32$ with FD > 0.6 mJy deg$^{-2}$.

TABLE 4
IDAS Asteroid Sightings

| Ast. | ID | R.A. | Decl. | S/N | Q1 | Q2 | Q3 | JD (−2,450,000) | C | FDCor | CorFD | RT |
|---|---|---|---|---|---|---|---|---|---|---|---|---|
| 1 | 3 | 339.575977 | −8.577812 | 25.1 | 1 | 1 | 4 | 249.79034 | 1 | 1.115 | 3926 | 17 |
| | 1008 | 339.588994 | −8.580972 | 17.2 | 3 | 4 | 4 | 249.89243 | 1 | 1.115 | 4225 | 17 |
| 2 | 4 | 339.647069 | −8.463253 | 22.0 | 0 | 4 | 4 | 249.78111 | 1 | 1.481 | 5580 | 17 |
| | 1003 | 339.672558 | −8.454937 | 24.3 | 0 | 4 | 4 | 249.88291 | 1 | 1.481 | 5559 | 17 |
| 3 | 5 | 339.595198 | −8.558890 | 14.8 | 3 | 4 | 4 | 249.78781 | 1 | 1.034 | 3111 | 17 |
| | 1015 | 339.596613 | −8.551524 | 13.3 | 2 | 2 | 4 | 249.89117 | 1 | 1.034 | 1997 | 17 |
| 4 | 35 | 339.754592 | −8.639367 | 6.6 | 4 | 4 | 4 | 249.77823 | 1 | 1.127 | 801 | 17 |
| | 1139 | 339.768698 | −8.638212 | 4.0 | 3 | 3 | 1 | 249.88102 | 1 | 1.127 | 542 | 17 |
| 5 | 43 | 339.700352 | −8.499148 | 6.3 | 4 | 4 | 4 | 249.77819 | 1 | 1.092 | 841 | 17 |
| | 1096 | 339.712344 | −8.497636 | 6.1 | 4 | 4 | 4 | 249.88087 | 1 | 1.092 | 597 | 17 |
| 6 | 55 | 339.651395 | −8.604998 | 7.4 | 4 | 4 | 4 | 249.78502 | 1 | 2.836 | 2022 | 17 |
| | 1184 | 339.702285 | −8.602760 | 4.1 | 4 | 4 | 1 | 249.88479 | 1 | 2.836 | 1231 | 17 |
| 7 | 85 | 339.715214 | −8.523705 | 4.5 | 4 | 4 | 1 | 249.77796 | 1 | 1.988 | 974 | 17 |
| | 1194 | 339.752778 | −8.528283 | 5.4 | 4 | 4 | 4 | 249.87869 | 1 | 1.988 | 908 | 17 |
| 8 | 94 | 339.630016 | −8.415515 | 4.5 | 0 | 4 | 1 | 249.78104 | 0 | 1.008 | 781 | 17 |
| | 1043 | 339.631924 | −8.418823 | 4.9 | 0 | 4 | 1 | 249.88402 | 0 | 1.008 | 857 | 17 |
| 9 | 111 | 339.634837 | −8.593815 | 5.0 | 4 | 4 | 3 | 249.78622 | 1 | 1.336 | 665 | 17 |
| | 1063 | 339.656464 | −8.587599 | 4.8 | 4 | 4 | 1 | 249.88802 | 1 | 1.336 | 698 | 17 |
| 10 | 230 | 339.647725 | −8.565410 | 5.9 | 4 | 4 | 4 | 249.78450 | 1 | 1.137 | 636 | 17 |
| | 1090 | 339.660784 | −8.558875 | 5.3 | 4 | 4 | 4 | 249.88686 | 1 | 1.137 | 690 | 17 |
| 11 | 4005 | 339.663681 | −8.665462 | 16.4 | 1 | 1 | 4 | 609.54157 | 1 | 1.266 | 2828 | 15 |
| | 5002 | 339.680263 | −8.658790 | 24.6 | 0 | 1 | 4 | 609.60102 | 1 | 1.266 | 4407 | 15 |
| | 8001 | 339.735623 | −8.635671 | 29.5 | 0 | 1 | 4 | 609.88002 | 1 | 1.295 | 5221 | 17 |
| | 9013 | 339.754758 | −8.626909 | 14.6 | 0 | 4 | 4 | 609.98160 | 1 | 1.295 | 2791 | 17 |
| 12 | 4018 | 339.647658 | −8.645995 | 10.2 | 3 | 3 | 4 | 609.54190 | 1 | 1.134 | 1141 | 15 |
| | 5028 | 339.659803 | −8.641898 | 7.8 | 0 | 3 | 3 | 609.60146 | 1 | 1.134 | 984 | 15 |
| | 8014 | 339.701216 | −8.625838 | 15.0 | 2 | 2 | 4 | 609.88251 | 1 | 1.159 | 1659 | 17 |
| | 9005 | 339.715405 | −8.619379 | 16.5 | 4 | 4 | 4 | 609.98432 | 1 | 1.159 | 2321 | 17 |
| 13 | 4022 | 339.672085 | −8.528938 | 7.4 | 3 | 3 | 4 | 609.53713 | 1 | 1.047 | 778 | 15 |
| | 5075 | 339.679506 | −8.526589 | 5.6 | 4 | 4 | 3 | 609.59736 | 1 | 1.047 | 961 | 15 |
| | 8016 | 339.699610 | −8.517709 | 9.7 | 4 | 4 | 4 | 609.87944 | 1 | 1.035 | 1154 | 17 |
| | 9025 | 339.706524 | −8.514754 | 8.5 | 3 | 3 | 4 | 609.98147 | 1 | 1.035 | 987 | 17 |
| 14 | 4024 | 339.761948 | −8.551948 | 6.4 | 4 | 4 | 4 | 609.53074 | 1 | 1.092 | 866 | 15 |
| | 5014 | 339.770892 | −8.545951 | 10.0 | 4 | 4 | 4 | 609.59120 | 1 | 1.092 | 1137 | 15 |
| | 9023 | 339.804980 | −8.513935 | 6.9 | 0 | 4 | 4 | 609.97516 | 0 | 1.092 | 1209 | 17 |
| 15 | 8161 | 339.809759 | −8.565357 | 4.7 | 0 | 4 | 1 | 609.87345 | 0 | 1.234 | 690 | 17 |
| | 9064 | 339.828591 | −8.565200 | 4.7 | 0 | 4 | 0 | 609.97520 | 0 | 1.234 | 713 | 17 |
| 16 | 4076 | 339.695200 | −8.541871 | 5.3 | 3 | 3 | 3 | 609.53601 | 1 | 1.106 | 652 | 15 |
| | 5135 | 339.706170 | −8.538451 | 4.2 | 4 | 4 | 1 | 609.59578 | 1 | 1.106 | 485 | 15 |
| | 8056 | 339.741951 | −8.523027 | 8.6 | 4 | 4 | 4 | 609.87615 | 1 | 1.115 | 826 | 17 |
| | 9045 | 339.754062 | −8.517344 | 4.8 | 4 | 4 | 1 | 609.97850 | 1 | 1.115 | 730 | 17 |
| 17 | 4119 | 339.630591 | −8.616134 | 4.3 | 4 | 4 | 1 | 609.54245 | 1 | 3.715 | 1609 | 15 |
| | 5219 | 339.655302 | −8.567826 | 4.5 | 4 | 4 | 1 | 609.59977 | 1 | 3.715 | 1523 | 15 |
| 18 | 4122 | 339.723015 | −8.643114 | 6.9 | 4 | 4 | 3 | 609.53682 | 1 | 1.149 | 762 | 15 |
| | 5051 | 339.736023 | −8.639538 | 7.0 | 0 | 4 | 4 | 609.59631 | 1 | 1.149 | 812 | 15 |
| | 8031 | 339.776996 | −8.625246 | 8.3 | 0 | 3 | 2 | 609.87701 | 1 | 1.174 | 870 | 17 |
| | 9174 | 339.792203 | −8.619354 | 4.3 | 0 | 4 | 1 | 609.97887 | 1 | 1.174 | 432 | 17 |
| 19 | 4137 | 339.700181 | −8.610512 | 4.1 | 4 | 4 | 1 | 609.53769 | 1 | 1.415 | 699 | 15 |
| | 5048 | 339.721199 | −8.604013 | 6.5 | 4 | 4 | 4 | 609.59626 | 1 | 1.415 | 930 | 15 |
| 20 | 8010 | 339.738208 | −8.687407 | 14.9 | 0 | 3 | 4 | 609.88123 | 0 | 1.727 | 5686 | 17 |
| | 9017 | 339.770672 | −8.684256 | 6.6 | 0 | 4 | 4 | 609.98219 | 0 | 1.727 | 2001 | 17 |

Singletons (i.e., a source detected only once) with flux densities above 0.6 mJy may also be present in these fields, but they cannot be unambiguously identified using these data alone.

### 4.2. *Known Asteroids Associated with IDAS Sources*

We associated known asteroids with two tracks found in the 1996 field. These were the only two known asteroids to appear in either field. Details on these sources are given in Table 5, where column (1) gives, as two rows per observation, the IDAS asteroid number assigned in Table 4 in the first row and the associated asteroid's designation in the second, column (2) gives the IDAS source number from Table 2, columns (3) and (4) give respectively the observed right ascension and declination in the first row and the predicted right ascension and declination, obtained using the HORIZONS software (Giorgini et al. 1996),[7] in the second row,

[7] The "HORIZONS On-Line Ephemeris System" was created and is maintained by the Solar System Dynamics Group, Jet Propulsion Laboratory (see http://ssd.jpl.nasa.gov/horizons.html).

TABLE 5

KNOWN ASTEROIDS IN THE 1996 JUNE 15 *ISO* FIELD

| (IDAS) Asteroid (1) | ID (2) | R.A. (deg) (3) | Decl. (deg) (4) | FD (μJy) (5) | S/N (6) | UTC (7) |
|---|---|---|---|---|---|---|
| (1)........................ | 3 | 339.57598 | −08.57781 | 4032 | 25.1 | 0658 |
| 1999 $AQ_{23}$........... | | 339.57288 | −08.57761 | | | |
| (1)........................ | 1008 | 339.58899 | −08.58097 | 4339 | 17.2 | 0925 |
| 1999 $AQ_{23}$........... | | 339.58596 | −08.58042 | | | |
| (2)........................ | 4 | 339.64707 | −08.46325 | 5543 | 22.0 | 0645 |
| 17971 1999 $JZ_{50}$.... | | 339.64713 | −08.46247 | | | |
| (2)........................ | 1003 | 339.67256 | −08.45494 | 5522 | 24.3 | 0911 |
| 17971 1999 $JZ_{50}$.... | | 339.67267 | −08.45481 | | | |

columns (5) and (6) the observed corrected flux density and S/N, respectively, and column (7) the UTC of the observation.

Of the 10 probable *ISO* asteroids identified in the 1996 field, those associated with 1999 $AQ_{23}$ and (17971) 1999 $JZ_{50}$ are the brightest. The predicted *V*-band magnitudes of these two asteroids at the time of the *ISO* observations were 18.2 and 18.1, respectively. This means that 80% of the asteroids in the 1996 field have $V > 18$, and for those with low albedos (0.03), the maximum *V* is about 24.

Figure 7 shows the observed *ISO*-centric positions for sources 3 and 1008 (1999 $AQ_{23}$) and sources 4 and 1003 ([17971] 1999 $JZ_{50}$) from the 1996 ISOCAM map, together with the *ISO*-centric positions for the two known asteroids. According to the HORIZONS documentation, " The database is updated almost daily with new objects and orbit solutions. Comet and asteroid orbits are integrated from initial conditions stored in the JPL-maintained DASTCOM database[8]." Because of the ephemeral nature of these orbital elements, we present in Table 6 those used in the analysis described here.

The ISOCAM coordinates, for the mean time of the extracted sources, are plotted in Figure 7 (*triangles*). Because the asteroid position is the mean from detections obtained over the ∼18 minutes required to map an inertial point on the sky, the predicted positions are shown as a series of 19 positions at 1 minute intervals centered on the midtime of the local map. The small squares centered on the predicted position trails are 6″ on a side, the size of an ISOCAM pixel used in this experiment, while the figure is ∼3′ on a side, the size of the ISOCAM array.

[8] See ftp://ssd.jpl.nasa.gov/pub/ssd/Horizons_doc.ps; version 2.80, 2000 June 14.

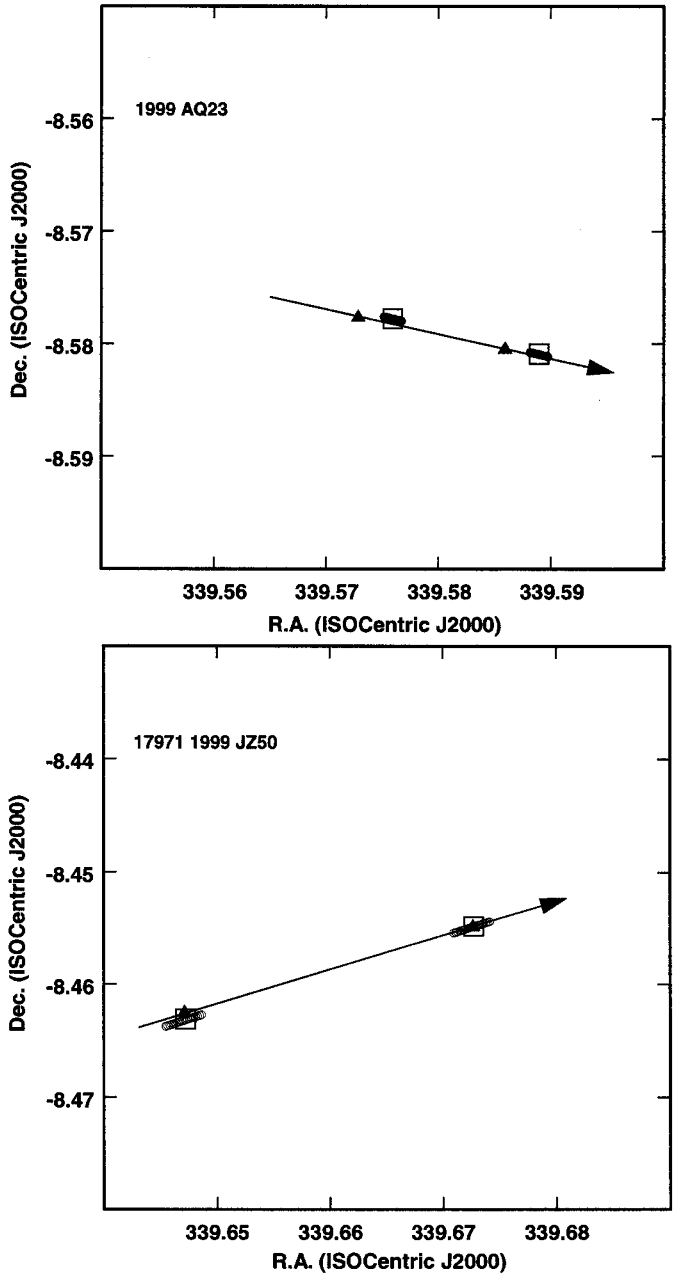


FIG. 7.—Observed (*circles*) vs. predicted (*triangles*) positions for two bright known asteroids in the 1996 *ISO* map. Each graph is 3′ on a side, the approximate size of the ISOCAM array. The small squares centered on the observed position are 6″ on a side, the approximate size of the ISOCAM PFOV used.

TABLE 6

HORIZONS INITIAL HELIOCENTRIC OSCULATING ELEMENTS[a]

| Asteroid | $T_p$ | $q$ | $e$ | AP | Ω | $i$ | $H$ |
|---|---|---|---|---|---|---|---|
| 1999 $AQ_{23}$.......... | 2,451,507.3543131 | 2.304351999 | 0.1217025 | 97.89149 | 135.42849 | 14.72242 | 13.5 |
| 17971 1999 $JZ_{50}$... | 2,451,472.0746345 | 1.887653106 | 0.168258407 | 167.6773526 | 128.5014528 | 2.9364673 | 14.8 |

NOTES.—$T_p$ = time of perihelion passage (Julian Date), $q$ = perihelion distance (AU), $e$ = eccentricity, AP = argument of perihelion (deg), Ω = longitude of the ascending node (deg), $i$ = inclination (deg), $H$ = absolute visual magnitude ($G$, the slope parameter, is assumed to be 0.15 for both asteroids). These data were obtained from Horizons on 2001 September 9.

[a] For ecliptic and mean equinox of J2000.0 and epoch = 2001 Oct 18.0000000 (TDB), for 1999 $AQ_{23}$ and 2001 Apr 01.0000000 (TDB), for 17971 1999 $JZ_{50}$.

TABLE 7
ASPECT DATA, FLUX, AND DERIVED DIAMETERS AND ALBEDOS FOR KNOWN ASTEROIDS ASSOCIATED WITH IDAS SOURCES

| Asteroid (1) | $V$ (mag) (2) | $H$ Dist. (AU) (3) | $G$ Dist. (AU) (4) | Phase (deg) (5) | Flux (mJy) (6) | D-STM (km) (7) | $p_H$-STM (8) | D-NEATM (km) (9) | $p_H$-NEATM (10) |
|---|---|---|---|---|---|---|---|---|---|
| 1999 $AQ_{23}$ .......... | 18.2 | 2.538 | 2.053 | 22.57 | $4.08 \pm 0.15$ | $2.80 \pm 0.02$ | $0.90 \pm 0.01$ | $3.30 \pm 0.02$ | $0.65 \pm 0.01$ |
| 17971 1999 $JZ_{50}$... | 18.1 | 1.892 | 1.333 | 31.01 | $5.57 \pm 0.01$ | $1.50 \pm 0.01$ | $0.93 \pm 0.01$ | $1.73 \pm 0.01$ | $0.71 \pm 0.01$ |
| Results Assuming Actual $H$ is 1 Full Magnitude Higher | | | | | | | | | |
| 1999 $AQ_{23}$ .......... | 19.2 | 2.538 | 2.053 | 22.57 | $4.08 \pm 0.15$ | $2.41 \pm 0.02$ | $0.48 \pm 0.01$ | $2.95 \pm 0.02$ | $0.32 \pm 0.01$ |
| 17971 1999 $JZ_{50}$... | 19.1 | 1.892 | 1.333 | 31.01 | $5.57 \pm 0.01$ | $1.30 \pm 0.01$ | $0.50 \pm 0.01$ | $1.54 \pm 0.01$ | $0.36 \pm 0.01$ |
| Results Assuming Actual $H$ is 0.5 mag Higher and Flux is a Factor of 1.5 Greater | | | | | | | | | |
| 1999 $AQ_{23}$ .......... | 18.7 | 2.538 | 2.053 | 22.57 | $6.12 \pm 0.15$ | $3.00 \pm 0.02$ | $0.51 \pm 0.01$ | $3.60 \pm 0.02$ | $0.34 \pm 0.01$ |
| 17971 1999 $JZ_{50}$... | 18.6 | 1.892 | 1.333 | 31.01 | $8.36 \pm 0.01$ | $1.60 \pm 0.01$ | $0.52 \pm 0.01$ | $1.90 \pm 0.01$ | $0.37 \pm 0.01$ |

The object 1999 $AQ_{23}$ moved a distance equivalent to the size of a pixel during the time required to complete the raster scan of its position, while (17971) 1999 $JZ_{50}$ moved about twice this distance. For the numbered asteroid, (17971) 1999 $JZ_{50}$, the difference between the observed ISOCAM positions and the predicted ephemeris positions are $2\farcs8$ and $0\farcs6$. For the unnumbered asteroid 1999 $AQ_{23}$, the observed positions lead[9] the predicted positions by about $11''$ (or 34 minutes in time).

As noted in § 3.2, the astrometric accuracy of the IDAS positions is better than $4''$ for 95% of the sources associating with USNO-A2.0 sources. The accuracy for moving sources is undoubtedly less, but probably not by a factor of 2–3. The formal accuracy of the asteroids' predicted positions is less than $1''$ (based upon output from the Lowell Observatory Asteroid Ephemeris (ASTEPH)[10] run on 2001 September 18).

Despite the relatively poor agreement in position for 1999 $AQ_{23}$, we nevertheless present the albedos and diameters for both 1999 $AQ_{23}$ and (17971) 1999 $JZ_{50}$ under the assumption that they are associated with the *ISO* sources indicated.

The results are presented in Table 7, where column (1) identifies the asteroid; columns (2)–(5) give the predicted visual magnitude, heliocentric distance, geocentric distance, and solar phase angle from the HORIZONS ephemerides for the midtime of the *ISO* observations; column (6), the corrected observed mean *ISO* LW10 band ($\sim$*IRAS*) 12 $\mu$m flux density and its uncertainty; columns (7) and (8), the computed diameter and geometric albedo using the standard thermal model (STM; Lebofsky et al. 1986), D-STM and $p_H$-STM, respectively; and columns (9) and (10), the computed diameter and geometric albedo using the Near-Earth Asteroid Thermal Model (NEATM; Harris 1998), D-NEATM and $p_H$-NEATM, respectively.

The results from the photometry are ambiguous. Using the given values for $H$ and the infrared fluxes, the derived geometric albedos, from either the STM or NEATM thermal model, are either unphysical ($\sim$0.9) or implausible ($\sim$0.65–0.71).

Physically plausible albedos can be obtained, for example, by assuming that $H$ for each of these asteroids is 1.0 mag higher than that published, or that $H$ is 0.5 mag larger and the 12 $\mu$m flux density is 50% higher than reported here, etc. (see Table 7). Changes of this magnitude for $H$ are not uncommon (see Tedesco et al. 2002b). In addition, a 50% underestimate of the *ISO* flux density is also possible. Furthermore, both of these asteroids are located in the inner part of the asteroid belt, where, at least for asteroids with diameters greater than $\sim$60 km, low-albedo asteroids make up less than 10% of the population (Gradie & Tedesco 1982). However, other than ruling out low albedos for these asteroids (because for the published values of $H$, albedos of 0.03 and 0.10 predict infrared flux densities of 290 and 84 mJy, respectively, using the STM and 194 and 56 mJy, respectively, using the NEATM, a factor of 10 to 50 higher than observed), an accurate albedo cannot be determined.

## 5. DISCUSSION

### 5.1. *The Sky-Plane Density*

There are $160 \pm 32$ asteroids per square degree at the ecliptic plane above the ISOCAM 12 $\mu$m band detection threshold of about 0.6 mJy and $80 \pm 16$ with flux densities greater than 1.0 mJy. For the fields observed in this experiment, the faintest asteroid source extracted has a flux density of $0.432 \pm 0.085$ mJy and $S/N = 4.3$. To put these results in perspective, *IRAS*'s 12 $\mu$m limiting sensitivity, for $S/N = 3$, was about 150 mJy, whereas most of the IDAS asteroids are between 150 and 350 times fainter.

The Statistical Asteroid Model (SAM; Tedesco et al. 2002a), created specifically to estimate the asteroid sky-plane density above a given flux limit for visual through infrared wavelengths, was run twice on a 4 $deg^2$ field ($1^\circ$ in latitude by $4^\circ$ in longitude) centered on the *ISO* field, once for the epoch of osculation of the model's orbital elements (1998 October 14) and a second time (yielding the results in parentheses in the following paragraph) for the date of the 1997 June *ISO* observations.

A total of 1063 (1638) of the approximately 2 million asteroids in the SAM were present in this 4 $deg^2$ field. Of these, 673 (852) had predicted 12 $\mu$m flux densities greater than 0.6 mJy. Thus, the model predicts $190 \pm 20$ asteroids per square degree with 12 $\mu$m flux densities greater than 0.6 mJy, in reasonable agreement with the *ISO* observations ($160 \pm 32$).

The SAM result is actually a lower limit because the model does not yet include near-Earth asteroids or asteroids

[9] The lead time is the difference between the time the known asteroid is closest to the position of the *ISO* source minus the time of the *ISO* observation of that source. The track of 1999 $AQ_{23}$, in *ISO*-centric coordinates, passes less than $1''$ from the observed positions.

[10] See http://asteroid.lowell.edu/cgi-bin/koehn/asteph; version 1.5.

beyond the Hilda group. More importantly, however, is the fact that it terminates abruptly at a diameter of 1 km. If smaller asteroids were included, some of these would have 12 $\mu$m flux densities greater than 0.6 mJy if they were close to Earth. Nevertheless, the *ISO* data imply that the actual number of kilometer-sized asteroids is in reasonable agreement (i.e., within $\sim$20%) with the number used in the SAM.

*SIRTF*'s imagers will have $\sim 5' \times 5'$ field-of-view arrays with 1″.2 pixels and sensitivities of $\sim$0.015 mJy at 8 $\mu$m and $\sim$0.37 mJy at 24 $\mu$m, about an order of magnitude more sensitive than the IDAS limit. Extrapolating the IDAS asteroid sky-plane density to a diameter of 0.316 km using the Durda, Greenberg, & Jedicke (1998) best-fit model, which gives 5 times as many asteroids at 0.316 km as at 1 km (see the following section for the details), and assuming that this value is correct to within a factor of 2 implies that an average of between three and 12 asteroids should appear in each limiting sensitivity *SIRTF* image. This estimate is independent of the actual *diameter* corresponding to 0.6 mJy, because it is an extrapolation of the observed sky plane density.

### 5.2. *The Main-Belt Asteroid Population*

An asteroid with a 12 $\mu$m *IRAS* flux density of 1 mJy at a heliocentric distance of 2.7 AU under the *ISO* observing geometry (an ecliptic latitude of 0° and solar elongation of 106°) would have a diameter of 1.25 km, and one with a flux density of 0.6 mJy a diameter of 1.0 km, using the same version of the STM used in reducing the *IRAS* data (Lebofsky et al. 1986)[11] and in creating the SAM (Tedesco et al. 2002a). These values for the diameters assume an albedo of 0.1178, the same used by Durda et al. (1998). In reality, at infrared wavelengths, the choice of albedo makes no significant difference, because (for the 0.6 mJy case) an albedo of 0.03 gives a diameter of 0.94 km, while an albedo of 0.36 gives 1.03 km. Thus, the uncertainty in the diameter due to assuming an albedo is about $^{+0.03}_{-0.06}$ km, i.e., about 5%. For a fixed albedo, 0.1178, the uncertainty due to the $\sim$0.6 AU uncertainty in the distances is about 55%.[12] In principle, heliocentric distances can be derived from the observed rates of motion. For example, Ivezić et al. (2001) demonstrate that, given positions accurate to better than 1″ and times accurate to better than a second, then, for asteroids observed not too far from opposition, heliocentric distances accurate to about 0.28 AU can be obtained. However, given that the IDAS fields were 74° from the opposition point, the astrometric accuracy no better than 4″, and the uncertainty in the time of observation on the order of a minute, we did not attempt to do so.

In this section, we use the term "population" to mean the number of main-belt asteroids with diameters greater than 1 km.

Assuming that the SAM population ($1.80 \times 10^6$) is a reasonable representation of the real main asteroid belt, using it to scale the observed IDAS sky-plane density gives a population estimate of $1.52 \times 10^6$ [i.e., $(160/190)1.80 \times 10^6$]. The formal uncertainty in this estimate is between 20% and 30%. Next, we compare this result with those from three recent studies based upon observations at visual wavelengths.

Evans et al. (1998) concluded from an analysis of 28,460 selected Wide Field Planetary Camera 2 visual-wavelength images that the 96 moving objects detected spanning the absolute magnitude range 13.6–19.3 (diameters between 7.4 and 0.5 km, assuming an albedo of 0.1178) implies the existence of $0.31 \times 10^6$ such asteroids within 25° of the ecliptic.

Using early results from the Sloan Digital Sky Survey, Ivezić et al. (2001) estimated the main-belt asteroid population to be $0.74 \times 10^6$. (This is the population after applying the factor of 1.1 to correct the result published for the sample completeness adjustment given in Ivezić et al.'s. note added in proof.)

Durda et al. (1998) converted the Jedicke & Metcalfe (1998) debiased absolute magnitude distribution to a size distribution by assuming that all asteroids smaller than the completeness limit of $\sim$30 km have the same albedo (0.1178). They refer to this as the "observed" size-frequency distribution; this bias-corrected estimated distribution extends to a diameter of 3 km. They then used this distribution to constrain a size-strength scaling relation for asteroidal strengths within their collisional model and then used that model to extrapolate the observed distribution to diameters less than $\sim$0.01 km. Although they do not present a population estimate, one can be deduced from their "best-fit model," an incremental size frequency distribution presented in their Figure 6*d*, a digitized version of which was provided by D. Durda (2001, private communication). The estimates presented here are based upon a log-log fit derived from the cumulative best-fit model for diameters between 2 and 0.2 km, viz.,

$$\log N_C = (5.9324 \pm 0.0016) - (1.5021 \pm 0045) \log D , \quad (2)$$

where $N_C$ is the cumulative number with diameters greater than $D$ kilometers.

The SAM and Durda et al. models are in good agreement for diameters greater than 2 km, at which size they give cumulative populations of $0.25 \times 10^6$ and $0.30 \times 10^6$, respectively. However, they diverge rapidly below this point, so that by 1 km (the lower diameter limit for SAM) the SAM versus Durda et al. population estimates are $1.80 \times 10^6$ and $0.86 \times 10^6$, respectively.

The formal uncertainty in each of the above estimates, based solely on counting statistics, is about 20%–30%, but systematic errors, for example, in converting magnitudes and fluxes to diameters, could raise this to perhaps 50%. If we take 25% as a crude "1 $\sigma$" uncertainty, the IDAS result is 0.7 $\sigma$ lower than the SAM estimate and 2.1, 2.6, and 4.4 $\sigma$ higher than the results of Durda et al. (1998), Ivezić et al. (2001), and Evans et al. (1998), respectively. If the actual 1 $\sigma$ uncertainties are 50%, then these differences become 0.4, 1.1, 1.3, and 2.2 $\sigma$, respectively.

If we give equal weights to the IDAS result and to the three estimates within 2 $\sigma$ (assuming 50% uncertainty is 1 $\sigma$) of the IDAS results, then the current "best estimate" for the number of main-belt asteroids with diameters greater than 1 km is $(1.2 \pm 0.5) \times 10^6$.

### 5.3. *Unknown Asteroids*

Despite the high quality of the *ISO* data, little can be said regarding the diameters (and nothing regarding the albedos)

[11] Using the NEA Thermal Model (Harris 1998) results in $\sim$18% larger diameters (cf. Table 7).

[12] If the heliocentric distance is 2.1 AU, the resultant STM diameter corresponding to a flux density of 0.6 mJy is 0.5 km; for a distance of 3.3 AU, it is 1.6 km.

of the individual unknown asteroids detected. This is because their orbits, and hence distances and phase angles, are unknown and cannot be reliably computed from the *ISO* positions alone. Reliable diameter determinations for these *ISO* asteroids will have to await their discovery. In addition, with *V* magnitudes probably fainter than 22 for most, this is unlikely to happen in the near future. Moreover, as illustrated in § 4.2, albedo determinations require, in addition to distance and phase information, reliable visual magnitudes.

Thus, in order to fully exploit space-based thermal infrared data, orbital elements of the asteroids observed must be known. In addition, if albedos are to be obtained, then visual wavelength observations are required as well. The minimum requirements for obtaining asteroid diameters in the absence of supporting ground-based observations is that the space-based data must simultaneously sample the asteroid's thermal spectrum at a minimum of three wavelengths bracketing the peak emission and be taken at appropriate intervals and with astrometric accuracies sufficient to allow computation of an approximate orbit.

NASA's Astrophysics Data Program supported E. T.'s portion of the work reported herein. E. T. gratefully acknowledges the support provided by Mary Ellen Barba, Ken Ganga, George Helou, Linda Hermans, Deborah Levine, Rosanne Scholley, Nancy Silbermann, Dave Van Buren, and Ann Wehrle in the planning, acquisition, and preliminary data reduction of the observations upon which this study was based. Thomas Mueller provided valuable input regarding associating *ISO* sources with known asteroids and directed E. T. to the HORIZONS system. E-mail exchanges with Dan Durda and Željko Ivezić helped nail down population estimates from their studies. The final version was improved based upon a review of the original manuscript by Clark Chapman.

## REFERENCES

Cesarsky, C. J., et al. 1996, A&A, 315, L32
Coulais, A., & Abergel, A. 2000, A&AS, 141, 533
Désert, F.-X., Puget, J.-L., Clements, D. L., Pérault, M., Abergel, A., Bernard, J.-P., & Cesarsky, C. J. 1999, A&A, 342, 363
Durda, D. D., Greenberg, R., & Jedicke, R. 1998, Icarus, 135, 431
Evans, R. W., et al. 1998, Icarus, 131, 261
Giorgini, J. D., et al. 1996, BAAS, 28, 1158
Gradie, J., & Tedesco, E. 1982, Science, 216, 1405
Harris, A. W. 1998, Icarus, 131, 291
Ivezić, Ž., et al. 2001, AJ, 122, 2749
Jedicke, R., & Metcalfe, T. S. 1998, Icarus, 131, 245
Kessler, M. F., et al. 1996, A&A, 315, L27
Lebofsky, L. A., et al. 1986, Icarus, 68, 239
Mill, J. D., et al. 1994, J. Spacecr. Rockets, 31, 900
Monet, D., et al. 1998, USNO-A2.0: A Catalogue of Astrometric Standards (Washington, D.C.: US Nav. Obs.)
Tedesco, E. F., ed. 1992, *IRAS* Minor Planet Survey (Phillips Lab. Tech. Rep. PL-TR-92-2049) (Hanscom AFB, MA: Phillips Lab., Dir. Geophys., Air Force Mater. Command)
Tedesco, E. F. 1994, in IAU Symp. 160, Asteroids, Comets, Meteors 1993, ed. A. Milani, M. di Martino, & A. Cellino (Dordrecht: Kluwer), 55
Tedesco, E. F., Cellino, A., & Zappalà, V. 2002a, in preparation
Tedesco, E. F., Egan, M. P., & Price, S. D. 2001, AJ, submitted
Tedesco, E. F., Noah, P. V., Noah, M., & Price, S. D. 2002b, AJ, 123, 1056